Eightfold Degenerate Fermions in Two Dimensions

Peng-Jie Guo,[1,2,*,†] Yi-Wen Wei,[1,2,*] Kai Liu,[3] Zheng-Xin Liu,[3,‡] and Zhong-Yi Lu[3]
[1]*Songshan Lake Materials Laboratory, Dongguan, Guangdong 523808, China*
[2]*Beijing National Laboratory for Condensed Matter Physics and Institute of Physics, Chinese Academy of Sciences, Beijing 100190, China*
[3]*Department of Physics and Beijing Key Laboratory of Opto-electronic Functional Materials & Micro-nano Devices, Renmin University of China, Beijing 100872, China*

(Received 20 May 2021; accepted 27 September 2021; published 22 October 2021)

Multifold degenerate fermions have attracted a lot of research interest in condensed matter physics and materials science, but always lack in two dimensions. In this Letter, from symmetry analysis and lattice model construction, we demonstrate that eightfold degenerate fermions can be realized in two-dimensional systems. In nonmagnetic materials with negligible spin-orbit coupling, the gray magnetic space groups together with SU(2) spin rotation symmetry can protect the two-dimensional eightfold degenerate fermions on a certain high-symmetry axis in the Brillouin zone, no matter whether the system is centrosymmetric or noncentrosymmetric. In antiferromagnetic materials, the eightfold degenerate fermions can also be protected by certain "spin space groups." Furthermore, by first-principles electronic structure calculations, we predict that the paramagnetic phase of the monolayer LaB_8 on a suitable substrate is a two-dimensional eightfold degenerate as well as Dirac node-line semimetal. Especially, the eightfold degenerate points are close to the Fermi level, which makes monolayer LaB_8 a good platform to study the exotic physical properties of two-dimensional eightfold degenerate fermions.

DOI: 10.1103/PhysRevLett.127.176401

Introduction.—In high-energy physics, relativistic massless Dirac fermions and Weyl fermions are the representations of the Poincaré group. At zero momentum, the massless Dirac fermions and Weyl fermions are four- and twofold degenerate, respectively. In condensed matter physics, the massless Dirac and Weyl fermions have been realized as the low-energy quasiparticle excitations [1–7]. The physical properties of massless Dirac and Weyl particles known in high-energy physics, such as the chiral anomaly, have also been observed in condensed matter physics [8,9]. On the other hand, 230 space groups are subgroups of the Poincaré symmetry; thus condensed matter systems have less constraints and new fermionic quasiparticles beyond high-energy physics can emerge [10–16]. For instance, three-, six-, and eightfold degenerate fermionic quasiparticles were proposed theoretically [10–16] and later realized in experiments [17,18]. So far, the new types of quasiparticles beyond the Dirac and Weyl fermions have been only studied in three-dimensional semimetals.

Two-dimensional (2D) systems contain rich physics in condensed matter. For instance, the first example of Dirac semimetal was realized in a 2D material—the graphene [19]. Furthermore, some special phenomena only exist in two dimensions (or at the surface of three-dimensional lattice systems), such as the integer and fractional quantum Hall effect and the quantum spin Hall effect [20–22]. In 2D systems, the point groups are uniaxial and the highest point group symmetry is D_{6h}. The relatively lowered symmetries thus strongly restrict the types of quasiparticles. For instance, the threefold degeneracy can never be protected in 2D materials since the uniaxial point groups do not have three-dimensional irreducible (projective) representations. The previously mentioned new types of nontrivial quasiparticles, if they exist in 2D, must be protected by nonsymmorphic space groups supporting layered structures.

In this Letter, based on group theory analysis and lattice model calculations, we demonstrate that the highest degeneracy of quasiparticles is eight, which is located on a high-symmetry line (HSL) in the Brillouin zone (BZ). Among the space groups supporting layered structures, four can protect eightfold degeneracy, including three centrosymmetric space groups (i.e., 51, 55, 127, with little cogroup $\mathscr{C}_{2v} \times \{E, \mathcal{IT}\}$, where $\mathcal{I}$ and $\mathcal{T}$, respectively, stand for space-inversion and time-reversal operation) and one noncentrosymmetric space group (i.e., 26 with little cogroup $2'm'm = \{E, C_{2x}\mathcal{T}, M_y\mathcal{T}, M_z\}$). More importantly, as long as the intrinsic spin-orbit coupling is negligible, the eightfold degenerate fermions can also stably exist in magnetic semimetals with collinear antiferromagnetic order, even if the Zeeman coupling between the spins of itinerary electrons and the local magnetic momentum essentially gives rise to spin-orbit coupling. These magnetic semimetals belong to two type-III magnetic space groups (51.293, 55.355) and six type-IV magnetic space groups (51.299, 51.300, 51.302, 55.360, 55.361, 127.396). Strictly speaking, in these systems, the magnetic space groups are enhanced to spin space groups in which the spin rotations are (partially) unlocked with the lattice rotations; accordingly the little cogroups of the HSLs are enhanced to a "spin point group" containing $\mathscr{C}_{2v} \times \{E, \mathcal{IT}\}$ as a subgroup (for details, see the Supplemental Material [23]). Finally, by first-principles electronic structure calculations, we predict that the monolayer LaB_8 on a suitable substrate is a 2D eightfold degenerate as well as Dirac node-line semimetal in paramagnetic phase.

Symmetry analysis.—Because of fractional translations associated with point-group operations, the little cogroup of some $\boldsymbol{k}$ points at the boundary of the BZ may have high-dimensional projective representations. These high-dimensional projective representations lead to extra degeneracies in the electronic energy band structure. There are a portion of the Dirac semimetals and Dirac node-line semimetals protected by nonsymmorphic space groups [39–43].

To understand the emergence of the eightfold degeneracy, we check the $P4/mbm$ (127) space group symmetry as an example. The elementary symmetry operations of the $P4/mbm$ space group include C_{4z}, $C_{2y}(1/2, 1/2, 0)$, and $\mathcal{I}$, which yield the point group D_{4h}. Since there is no fractional translation along the z direction, the space group $P4/mbm$ can support quasi-2D lattice structure. In the following, our discussion is restricted to the xy plane with the BZ shown in Fig. 1(a). Obviously, any $\boldsymbol{k}$ point on the X_x-M line is invariant under the following symmetry operations: the screw rotation $C_{2y}(1/2,1/2){:}(x,y) \to (-x+1/2, y+1/2)$, the glide mirror $M_x(1/2,1/2){:}(x,y) \to (-x+1/2, y+1/2)$, and the mirror $M_z{:}(x,y) \to (x,y)$. Furthermore, since $\mathcal{T}$ is always a symmetry element of nonmagnetic materials, the X_x-M line is also invariant under the combined symmetry operations $\mathcal{IT}$. Noticing that the square of the symmetry operation $C_{2y}(1/2, 1/2)\mathcal{IT} = M_y(1/2, 1/2)\mathcal{T}$ is $[M_y(1/2, 1/2)\mathcal{T}]^2 = (1, 0)$, the square of the representation of $M_y(1/2, 1/2)\mathcal{T}$ is equal to -1, resulting in a Kramers degeneracy in the energy spectrum. In other words, the fractional translations of the nonsymmorphic group give rise to two-dimensional irreducible projective representations of the little cogroup of the X_x-M line, i.e., $\mathscr{C}_{2v} \times Z_2^{\mathcal{IT}}$ with $\mathscr{C}_{2v} = \{E, C_{2y}, M_x, M_z\}$ and $Z_2^{\mathcal{IT}} = \{E, \mathcal{IT}\}$. This projective representation makes X_x-M a nodal line [see Fig. 1(b)].

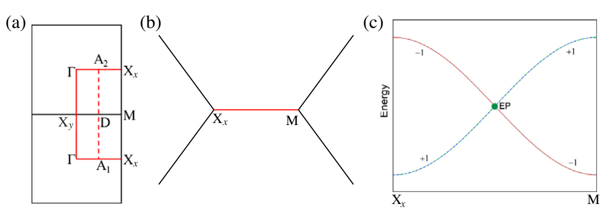

FIG. 1. (a) The BZ of square lattice. Schematic illustration for generation of (b) a Dirac nodal line and (c) eightfold degenerate point for $P4/mbm$ space group. The "EP" represents eightfold degenerate point.

On the other hand, since $M_y(1/2, 1/2)\mathcal{T}$ commutes with M_z, the X_x-M axis has two inequivalent Kramers pairs distinguished by the quantum number ± 1, the eigenvalues of M_z. This can be seen more clearly from the character table (Table I) of the unitary part of the little cogroup $\mathscr{C}_{2v}$ and the action of the antiunitary operation $\mathcal{IT}$. Obviously, the two one-dimensional irreducible representations $D^{(1)}$ and $D^{(2)}$ form a Kramers pair, while $D^{(3)}$ and $D^{(4)}$ form another Kramers pair. Because of different quantum numbers of M_z, the two Kramers pairs are not equivalent; also see the group theory analysis in the Supplemental Material [23].

If a band with the first Kramers pair crosses another band with the second Kramers pair, a pair of crossing points are formed on the X_x-M axis, as shown in Fig. 1(c). On the other hand, since spin-orbital coupling is not taken into account, the spin space has SU(2) symmetry, which protects the spin degeneracy. Therefore, the pair of crossing points are eightfold degenerate. Because of the C_{4z} symmetry, another pair of eightfold degenerate points can be found on the X_y-M axis.

Interestingly, even if the $\mathcal{I}$ (and hence $\mathcal{IT}$) is broken, the $M_y(1/2, 1/2)\mathcal{T}$ symmetry still protects the Kramers pairs on the X_x-M axis and the quantum number of M_z symmetry still guarantees that there are two inequivalent Kramers pairs. Hence, even when the little cogroup reduces to $2'm'm = \{E, M_y\mathcal{T}, M_z, C_{2x}\mathcal{T}\} \times \mathrm{SU}(2)$ owing to the missing central inversion, the Dirac nodal-line structure and the eightfold degenerate points on the X_x-M axis are still protected. However, since C_{4z} and $M_x(1/2, 1/2)\mathcal{T}$ are no longer symmetry operations, the Dirac nodal line is lifted on the X_y-M axis and the eightfold degenerate points split into several cones with lower degeneracy.

Effective lattice model.—Here we provide a lattice model to illustrate the eightfold degeneracy protected by the $P4/mbm$ space group symmetry. The minimal model is on a square lattice including four sublattices, as shown in Fig. 2(a). We begin with a Hamiltonian composed of s orbitals, including the hopping between the nearest and next-nearest neighbors as follows:

$$\begin{aligned} h_{\boldsymbol{k}} = {} & t(1+\cos k_x)\Sigma_{01} + t\sin k_x\Sigma_{32} + t(1+\cos k_y)\Sigma_{11} \\ & - t\sin k_y\Sigma_{21} + t'/2[1+\cos(k_x+k_y)]\Sigma_{10} \\ & + t'/2[1-\cos(k_x+k_y)]\Sigma_{13} \\ & - t'/2\sin(k_x+k_y)(\Sigma_{20}-\Sigma_{23}), \end{aligned} \tag{1}$$

TABLE I. Character table of $\mathscr{C}_{2v}$ group at the X_x-M axis.

C_{2v}	E	$C_{2y}(1/2, 1/2)$	M_z	$M_x(1/2, 1/2)$
$D^{(1)}$	1	$-i$	1	$-i$
$D^{(2)}$	1	i	1	i
$D^{(3)}$	1	$-i$	-1	$-i$
$D^{(4)}$	1	i	-1	i

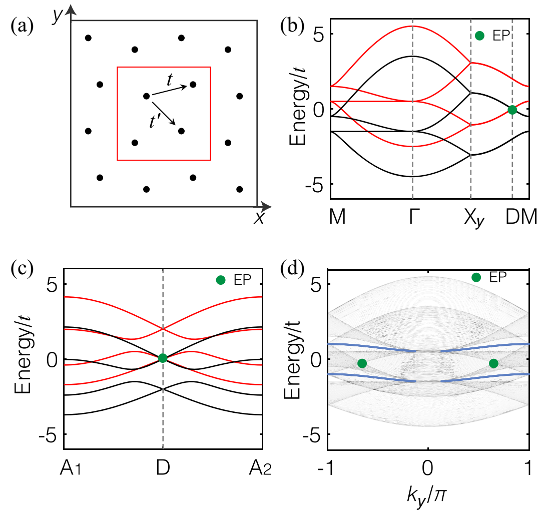

FIG. 2. Energy bands for the lattice model with eightfold degenerate points under the $P4/mbm$ group. (a) A schematic representation of the square lattice with the nearest and next-nearest neighbor hopping integrals. The red square marks the unit cell. (b),(c) The band structures of lattice model along the high-symmetry directions. (d) Energy spectrum for a nanoribbon with 60 unit cells in the x direction and infinite along the y direction. The red (black) bands represent the mirror M_z eigenvalue $1(-1)$. The edge states are labeled by blue. The eightfold degenerate points are marked by green dots.

where $\Sigma_{ij} = s_i \otimes s_j$ describes the sublattice degrees of freedom, s_0 is the 2×2 identity matrix, s_1, s_2, and s_3 are the Pauli matrices, and t and t' are the nearest neighbor and next-nearest neighbor hopping integrals, respectively. It is obvious that the system preserves both $\mathcal{T}$ and $\mathcal{I}$ symmetry. The spin index is omitted since spin-orbital coupling is ignored. According to the above symmetry analysis, the eightfold degenerate points are formed by the crossing of two Kramers bands with different quantum numbers labeled by the eigenvalues of M_z. Since the s orbitals carry quantum $+1$ of M_z, the p_z orbitals should be included in the Hamiltonian, yielding

$$H_{\boldsymbol{k}} = h_{\boldsymbol{k}} + m\tau_3, \tag{2}$$

where the Pauli matrix τ_3 acts on the orbital degree of freedom.

The band structure with parameters $t = 2t' = m = 1$ is shown in Figs. 2(b) and 2(c). We can see a double degeneracy in addition to spin degeneracy on the X_y-M line, which is protected by the $M_x(1/2,1/2)\mathcal{T}$ symmetry. As expected, the eightfold degenerate point is generated by the crossing energy bands with different quantum numbers of M_z. We also calculated the edge sates at the open boundaries in the x direction. As shown in Fig. 2(d), there are no edge states connecting the two eightfold degenerate points, which is different from the Dirac semimetals caused by band inversion [2,3].

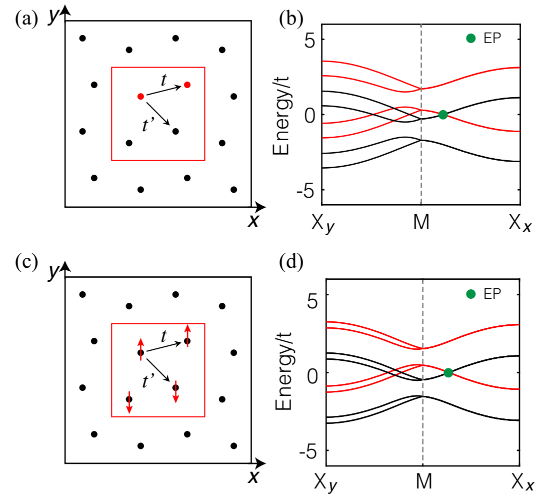

FIG. 3. Lattice model and bands structures. (a), (b) Breaking $\mathcal{I}$ symmetry. (c),(d) Breaking $\mathcal{I}$ and $\mathcal{T}$ symmetry with an out-of plane antiferromagnetic order. The red (black) bands represent the mirror M_z eigenvalue $1(-1)$. The eightfold degenerate points are marked by green dots. The red arrows represent magnetic moment.

Furthermore, we break $\mathcal{I}$ symmetry by distinguishing the red and black sites in Fig. 3(a) by adding an on-site different potential energy on the red and black sites in Fig. 3(a), namely, $t_0\Sigma_{30}$ in the Hamiltonian. Now the new Hamiltonian $H'_{\boldsymbol{k}} = H_{\boldsymbol{k}} + t_0\Sigma_{30}$ preserves $C_{2x}(1/2,1/2)\mathcal{T}$, $M_y(1/2,1/2)\mathcal{T}$, and M_z symmetries. As expected, the eightfold degenerate point on the X_y-M axis is lifted, but the one on the X_x-M axis remains, as shown in Fig. 3(b) plotted with $t_0 = 0.5t$. Thus the 2D eightfold degenerate semimetals can stably exist in noncentrosymmetric systems.

Now we provide all the space groups that can protect the eightfold degeneracy in 2D semimetals. First, there are only 17 nonsymmorphic space groups supporting 2D layered structures as listed in Table II, which may protect 2D eightfold degenerate fermions. Second, we have just shown that with extra SU(2) spin rotation symmetry there are two kinds of little cogroups that can protect the eightfold degeneracy, namely, $\mathscr{C}_{2v}\times Z_2^{\mathcal{I}\mathcal{T}}$ and $2'm'm$. Since time reversal $\mathcal{T}$ is always a symmetry of the system, the unitary point group of the required space group

TABLE II. The relationship of two-dimensional nonsymmorphic space group and eightfold degenerate semimetals.

Point group	Space groups	Eightfold degeneracy
C_{2v}	26	Yes
C_{2v}	27,28,29,30,31	No
D_{2h}	49,50,53,54,57,59	No
D_{2h}	51,55	Yes
D_{4h}	125,129	No
D_{4h}	127	Yes

should contain $\mathscr{C}_{2v} \times \{E, \mathcal{I}\} = D_{2h}$ (if $\mathcal{I}$ is present) or $\mathscr{C}_{2v} = \{E, M_y, M_z, C_{2x}\}$ (if $\mathcal{I}$ is absent) as its subgroup. It turns out that all of the 17 space groups satisfy the second requirement.

Third, the fractional translation associated with the little cogroup elements (on a HSL) should support two inequivalent Kramers degeneracies. The Kramers degeneracy can be protected by one of the following symmetry elements: $M_x(1/2, 1/2)\mathcal{T}$, $M_x(0, 1/2)\mathcal{T}$, $C_{2x}(1/2, 1/2)\mathcal{T}$, $C_{2x}(1/2, 0)\mathcal{T}$, $M_y(1/2, 1/2)\mathcal{T}$, $M_y(1/2, 0)\mathcal{T}$, $C_{2y}(1/2, 1/2)\mathcal{T}$, or $C_{2y}(0, 1/2)\mathcal{T}$. We further need the operation M_z to provide the quantum numbers ± 1 to distinguish two inequivalent Kramers pairs. It turns out that only four space groups (51, 55, 127, and 26) satisfy the above requirements, as shown in Table II. Different from the 127 ($P4/mbm$) space group, the eightfold degenerate points protected by the 26(P-$mc21$) or the 51(P-mma) space group can only locate at one boundary axis of the 2D BZ. The 55(P-bam) space group is special, the eightfold degenerate points can locate at either one or two boundary axes in the 2D BZ.

Finally, we consider an out-of-plane collinear antiferromagnetic order that breaks the $\mathcal{I}$ and $\mathcal{T}$ symmetry but preserves the combined $\mathcal{I}\mathcal{T}$ symmetry, as shown in Fig. 3(c). Then the new Hamiltonian becomes $H'_{\boldsymbol{k}} = H_{\boldsymbol{k}} + 2t_m \Sigma_{30}(\sigma_z/2)$ (the second term is the Zeeman coupling between the local magnetic momentum and electron spin, with $(\sigma_z/2)$ the z component spin operator). While the Zeeman term introduces spin-orbit coupling to the Hamiltonian, the operations $C_{2y}(1/2, 1/2)$, $M_x(1/2, 1/2)$, M_z, and $\mathcal{I}\mathcal{T}$ remain to be symmetries of the Hamiltonian $H'_{\boldsymbol{k}}$ if each operation is interpreted as a combination of lattice operation and the corresponding spin rotation. If the intrinsic kinetic term $H_{\boldsymbol{k}}$ has negligible spin-orbit coupling, then the total Hamiltonian $H'_{\boldsymbol{k}}$ has extra symmetries since the system is invariant under spin rotation $(C_{2z}||E)$ and lattice mirror reflection $(E||M_z)$ (here C_{2z} acts on spin only, while M_z acts on lattice only). In other words, the little cogroup on the X_x-M line is enlarged into a spin point group containing the Shubnikov magnetic point group $\mathscr{C}_{2v} \times Z_2^{\mathcal{I}\mathcal{T}}$ as a subgroup. This spin point group can protect the eightfold degenerate points on the X_x-M axis (see the Supplemental Material [23] for details). The dispersion of a lattice model with $t_m = 0.2t$ is shown in Fig. 3(d). Notice that the eightfold degenerate point on the X_y-M axis is lifted due to the absence of $C_{2x}(1/2, 1/2)$ and $M_y(1/2, 1/2)$ symmetry as shown in Fig. 3(d).

Therefore, the sufficient conditions of the eightfold degeneracy include the following: (1) the system contains out-of plane collinear antiferromagnetic order, (2) the intrinsic spin-orbit coupling for the electrons is negligible, and (3) the Shubnikov little cogroup on a high-symmetry line is $\mathscr{C}_{2v} \times Z_2^{\mathcal{I}\mathcal{T}}$. It turns out that only eight magnetic space groups satisfy the above condition, including two type-III magnetic space groups (51.293, 55.355) and six type-IV magnetic space groups (51.299, 51.300, 51.302, 55.360, 55.361, 127.396).

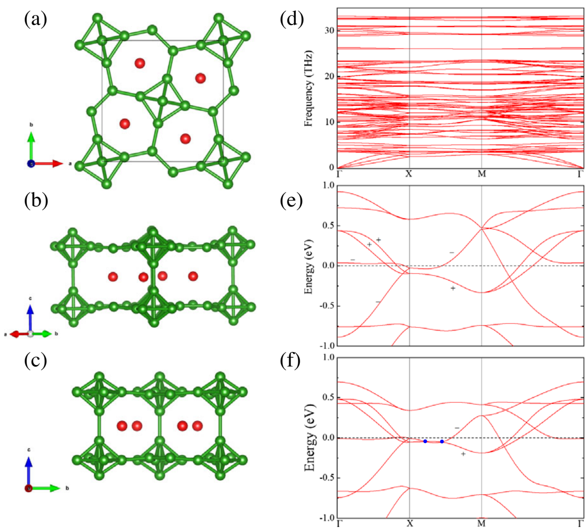

FIG. 4. Crystal structure of monolayer LaB_8 viewed along (a) [100], (b) [110], and (a) [001] directions. The red and green balls represent La and B atoms, respectively. (d) Phonon spectrum of monolayer LaB_8 along the high-symmetry directions. The electronic band structures of monolayer LaB_8 along the high-symmetry directions for (e) relaxed crystal structure and (f) compressing the lattice constant by 3%. The "+" and "−" represent the eigenvalue of mirror M_z with 1 and -1, respectively. The eightfold degenerate points are marked by blue dots.

Material calculations.—In terms of realistic materials, since 2D eightfold degenerate semimetals are fragile when considering spin-orbit coupling (SOC), we can find 2D eightfold degenerate semimetals in layered light element compounds. Here, we propose a new 2D structure LaB_8, which is constructed from the bulk LaB_4 [44] under space group $P4$-mbm. The monolayer LaB_8 is made up of two layers of B atoms and one layer of La atoms as shown in Figs. 4(a)–4(c). The B atomic layer is made up of B atomic octahedron and B atoms [Fig. 4(a)].

In order to confirm the structural stability, we calculated the phonon spectrum of monolayer LaB_8 as shown in Fig. 4(d). Clearly, the phonon spectrum of monolayer LaB_8 has no imaginary frequency, thus the crystal structure is dynamically stable. As shown in Fig. 4(e), the electronic band structure of monolayer LaB_8 has six Dirac nodal lines around the Fermi level, which can be divided into two kinds. One kind derives from the band inversion around the time-reversal invariant Γ point and is protected by the mirror symmetry M_z, while the other one must be in the X-M axis and is protected by nonsymmorphic symmetry as the above symmetry analysis. Without strain, the monolayer LaB_8 unfortunately does not support the eightfold degenerate fermions. But the two Dirac nodal lines along the X-M direction have different quantum numbers of M_z and are very close around the high-symmetry point X [Fig. 4(e)]. By applying lattice strain, the nodal lines could probably touch each other and produce the eightfold degenerate points. When compressing the lattice constant by 3%, the nonmagnetic state of a monolayer LaB_8 indeed contains eightfold degenerate fermions as shown in Fig. 4(f). Although the stressed LaB_8 actually exhibits ferromagnetic order at zero temperature, it is argued in the Supplemental Material [23] that the eightfold degenerate fermions still exist at finite temperatures. Because of the C_4 rotation symmetry, the monolayer LaB_8 has eight eightfold degenerate points. Moreover, since the SOC has very weak influence on the bands around the Fermi level [23], the monolayer LaB_8 on a suitable substrate may be an ideal platform for studying the exotic properties of 2D eightfold degenerate fermions in the paramagnetic phase.

In summary, based on symmetry analysis, lattice model, and the first-principles electronic calculations, we obtain five main results: (i) The eightfold degenerate fermions can stably exist in 2D systems. (ii) The little cogroups $\mathscr{C}_{2v} \times \{E, \mathcal{IT}\}$ and $2'm'm = \{E, C_{2x}\mathcal{T}, M_y\mathcal{T}, M_z\}$ on a certain HSL in the Brillouin zone can protect the 2D eightfold degenerate fermions in centrosymmetric or noncentrosymmetric nonmagnetic systems, respectively. (iii) There are four space groups that can protect eightfold degenerate fermions, including three centrosymmetric space groups (51, 55, 127) and one noncentrosymmetric space group (26). (iv) As long as the intrinsic spin-orbit coupling is negligible, the eightfold degenerate fermions can also stably exist in magnetic semimetals with collinear antiferromagnetic order belonging to two type-III magnetic space groups (51.293, 55,355) and six type-IV magnetic space groups (51.299, 51.300, 51.302, 55.360, 55.361, 127.396), even if the Zeeman coupling between the spins of itinerant electrons and the local magnetic momentum actually contains spin-orbit coupling. (v) The monolayer LaB_8 on a suitable substrate may well be a platform for studying the exotic properties of 2D eightfold degenerate fermions.

We thank H.-M. Weng, J. Yang, and C. Fang for helpful discussions. P.-J. G. was supported by the fellowship of China Postdoctoral Science Foundation (Grant No. 2020TQ0347). Y.-W. W. was supported by Guangdong Basic and Applied Basic Research Foundation (Grant No. 2020A1515111196). K. L. was supported by the National Natural Science Foundation of China (Grant No. 11774424). Z. X. L. was supported by the NSF of China (No. 11974421 and No. 12134020) and the State Key Program of the National Natural Science Foundation of China (No. 12134020). The computational resource was provided by the Platform for Data-Driven Computational Materials Discovery of the Songshan Lake Laboratory.

[*]These authors have contributed equally to this work.
[†]pjguo@iphy.ac.cn
[‡]liuzxphys@ruc.edu.cn

[1] X. G. Wan, A. M. Turner, A. Vishwanath, and S. Y. Savrasov, Phys. Rev. B **83**, 205101 (2011).
[2] Z. J. Wang, Y. Sun, X. Q. Chen, C. Franchini, G. Xu, H. M. Weng, X. Dai, and Z. Fang, Phys. Rev. B **85**, 195320 (2012).
[3] Z. J. Wang, H. M. Weng, Q. S. Wu, X. Dai, and Z. Fang, Phys. Rev. B **88**, 125427 (2013).
[4] Z. K. Liu, B. Zhou, Y. Zhang, Z. J. Wang, H. M. Weng, D. Prabhakaran, S.-K. Mo, Z. X. Shen, Z. Fang, X. Dai, Z. Hussain, and Y. L. Chen, Science **343**, 864 (2014).
[5] Z. K. Liu, J. Jiang, B. Zhou, Z. J. Wang, Y. Zhang, H. M. Weng, D. Prabhakaran, S.-K. Mo, H. Peng, P. Dudin, T. Kim, M. Hoesch, Z. Fang, X. Dai, Z. X. Shen, D. L. Feng, Z. Hussain, and Y. L. Chen, Nat. Mater. **13**, 677 (2014).
[6] H. Weng, C. Fang, Z. Fang, B. A. Bernevig, and X. Dai, Phys. Rev. X **5**, 011029 (2015).
[7] H. M. Weng, X. Dai, and Z. Fang, J. Phys. **28**, 303001 (2016).
[8] J. Xiong, S. K. Kushwaha, T. Liang, J. W. Krizan, M. Hirschberger, W. D. Wang, R. J. Cava, and N. P. Ong, Science **350**, 413 (2015).
[9] X. C. Huang, L. X. Zhao, Y. J. Long, P. P. Wang, D. Chen, Z. H. Yang, H. Liang, M. Q. Xue, H. M. Weng, Z. Fang, X. Dai, and G. F. Chen, Phys. Rev. X **5**, 031023 (2015).
[10] B. J. Wieder, Y. Kim, A. M. Rappe, and C. L. Kane, Phys. Rev. Lett. **116**, 186402 (2016).
[11] B. Bradlyn, J. Cano, Z. J. Wang, M. G. Vergniory, C. Felser, R. J. Cava, and B. A. Bernevig, Science **353**, 6299 (2016).
[12] H. M. Weng, C. Fang, Z. Fang, and X. Dai, Phys. Rev. B **93**, 241202(R) (2016).
[13] H. M. Weng, C. Fang, Z. Fang, and X. Dai, Phys. Rev. B **94**, 165201 (2016).
[14] G. Q. Chang, S. Y. Xu, B. J. Wieder, D. S. Sanchez, S. M. Huang, I. Belopolski, T. R. Chang, S. T. Zhang, A. Bansil, H. Lin, and M. Z. Hasan, Phys. Rev. Lett. **119**, 206401 (2017).
[15] P. Z. Tang, Q. Zhou, and S. C. Zhang, Phys. Rev. Lett. **119**, 206402 (2017).
[16] P. J. Guo, H. C. Yang, K. Liu, and Z. Y. Lu, Phys. Rev. B **98**, 045134 (2018).
[17] B. Q. Lv, Z. L. Feng, Q. N. Xu, X. Gao, J. Z. Ma, L. Y. Kong, P. Richard, Y. B. Huang, V. N. Strocov, C. Fang, H. M. Weng, Y. G. Shi, T. Qian, and H. Ding, Nature (London) **546**, 627 (2017).
[18] Z. Rao, H. Li, T. Zhang, S. Tian, C. Li, B. Fu, C. Tang, L. Wang, Z. Li, W. Fan, J. Li, Y. Huang, Z. Liu, Y. Long, C. Fang, H. Weng, Y. Shi, L. H., Y. Sun, T. Qian, and H. Ding, Nature (London) **567**, 496 (2019).
[19] A. H. Castro Neto, F. Guinea, N. M. R. Peres, K. S. Novoselov, and A. K. Geim, Rev. Mod. Phys. **81**, 109 (2009).
[20] K. v. Klitzing, G. Dorda, and M. Pepper, Phys. Rev. Lett. **45**, 494 (1980).
[21] H. L. Stormer, D. C. Tsui, and A. C. Gossard, Rev. Mod. Phys. **71**, S298 (1999).
[22] C. L. Kane and E. J. Mele, Phys. Rev. Lett. **95**, 146802 (2005).
[23] See Supplemental Material at http://link.aps.org/supplemental/10.1103/PhysRevLett.127.176401 for details of the representations of the symmetry group and the stability of the eight-fold degeneracy, which includes Refs. [24–38].

[24] J. Yang, C. Fang, and Z. X. Liu, Phys. Rev. B **103**, 245141 (2021).
[25] D. P. Guo, P. J. Guo, S. L. Tan, M. Feng, L. M. Cao, Z. X. Liu, K. Liu, Z.-Y. Lu, and W. Ji, arXiv:2012.15218.
[26] X. X. Cui, Y. F. Li, D. P. Guo, P. J. Guo, C. C. Lou, G. Q. Mei, C. Lin, S. J. Tan, Z. X. Liu, K. Liu, Z. Y. Lu, H. Petek, L. M. Cao, W. Ji, and M. Feng, arXiv:2012.15220.
[27] D. B. Litvin and W. Opechowski, Physica (Utrecht) **76**, 538 (1974).
[28] J. Yang, Z. X. Liu, and C. Fang, arXiv:2105.12738.
[29] D. B. Litvin, Acta Cryst. A **33**, 279 (1977).
[30] Z. Y. Yang, J. Yang, C. Fang, and Z. X. Liu, J. Phys. A **54**, 265202 (2021).
[31] C. Si, Z. M. Sun, and F. Liu, Nanoscale **8**, 3207 (2016).
[32] P. E. Blöchl, Phys. Rev. B **50**, 17953 (1994).
[33] G. Kresse and D. Joubert, Phys. Rev. B **59**, 1758 (1999).
[34] G. Kresse and J. Hafner, Phys. Rev. B **47**, 558 (1993).
[35] G. Kresse and J. Furthmüller, Comput. Mater. Sci. **6**, 15 (1996).
[36] G. Kresse and J. Furthmüller, Phys. Rev. B **54**, 11169 (1996).
[37] J. P. Perdew and K. Burke, and M. Ernzerhof, Phys. Rev. Lett. **77**, 3865 (1996).
[38] A. Togo and I. Tanaka, Scr. Mater. **108**, 1 (2015).
[39] S. M. Young, S. Zaheer, J. C. Y. Teo, C. L. Kane, E. J. Mele, and A. M. Rappe, Phys. Rev. Lett. **108**, 140405 (2012).
[40] S. M. Young and C. L. Kane, Phys. Rev. Lett. **115**, 126803 (2015).
[41] S. Guan, Y. Liu, Z. M. Yu, S. S. Wang, Y. G. Yao, and S. Y. A. Yang, Phys. Rev. Mater. **1**, 054003 (2017).
[42] X. T. Fan, D. S. Ma, B. T. Fu, C. C. Liu, and Y. G. Yao, Phys. Rev. B **98**, 195437 (2018).
[43] W. K. Wu, Y. L. Jiao, S. Li, X. L. Sheng, Z. M. Yu, and S. Y. A. Yang, Phys. Rev. Mater. **3**, 054203 (2019).
[44] J. A. Deacon and S. E. R. Hiscocks, J. Mater. Sci. **6**, 309 (1971).